



## Thin film diamond membranes bonded on-demand with SOI ring resonators

Paul Hill<sup>a,b,\*</sup>, Erdan Gu<sup>a</sup>, Martin D. Dawson<sup>a</sup>, Michael J. Strain<sup>a</sup>

<sup>a</sup> Institute of Photonics, University of Strathclyde, Technology and Innovation Centre, University of Strathclyde, 99 George St., Glasgow G1 1RD, United Kingdom of Great Britain and Northern Ireland

<sup>b</sup> Diamond Science and Technology, Centre for Doctoral Training, University of Warwick, Gibbet Hill Road, Coventry CV4 7AL, United Kingdom of Great Britain and Northern Ireland

### ABSTRACT

The hybrid integration of single-crystal (SC) diamond membranes with on-chip optical devices has the potential to service many applications, spanning non-linear optics to quantum photonics with embedded diamond colour centres. Limited dimensions of high optical quality diamond however restrict the size and number of devices that can be fabricated on a single chip, which impedes the use of diamond in large photonic integrated circuitry. Here we show the fabrication and integration of a 1 μm thick SC diamond membrane with a silicon photonic device. The quality of the diamond-silicon interface is measured using SEM and optical techniques. Silicon microring resonators are measured after integration with the diamond film and show a low excess loss of 0.4 dB and a group index dispersion that is dependent on the mode confinement in the diamond layer.

### 1. Introduction

Diamond is attractive as a material for use in high-performance on-chip photonic devices. It boasts a large Raman gain ( $\sim 10$  cm/GW @ 1 μm), a wide bandgap (5.5 eV @ RT), and impressive thermal properties such as its high thermal conductivity ( $2 \times 10^3$  Wm<sup>-1</sup> K<sup>-1</sup>) and small thermo-optic coefficient ( $\sim 10^{-5}$  K<sup>-1</sup>) [1,2]. It has a large Kerr non-linearity and also plays host to several promising defect centres. The large bandgap of diamond corresponds to a transparency spanning ultraviolet wavelengths into the deep infrared, and its high refractive index of  $\sim 2.4$  gives good optical confinement and thus enables nanoscale photonic structures. Current single crystal diamond material is only available in small mm scale pieces, making fabrication of monolithic large scale integrated circuits a significant challenge. To harness diamond for integrated photonic applications, a method by which thin film material can be integrated with other optical devices is required. In this work we present a hybrid integration technique based on the bonding of a flexible diamond platelet to pre-fabricated integrated photonic devices on a different material. The host devices in this work are fabricated on the silicon platform. The well-established characteristics of silicon photonic devices allow the probing of the diamond-silicon bond interface. Nevertheless, the method is equally applicable across a wide range of material platforms. The choice of host integrated photonic platform will be dictated by the target application, for example, silicon may be used for non-linear optical applications in the telecommunications and Mid-IR bands [2-4], whilst a range of III-V

semiconductors or SiN, which are transparent in the visible and near-IR, would be compatible with coupling to diamond colour centres for quantum applications [5-8]. Integration of diamond with established photonic circuitry is limited due to the difficulty with which it is processed. Many recent efforts have been made such as by fabricating thin GaP membranes and then transferring them to bulk diamond where single mode resonators are then fabricated [8-11]. GaP presents a high refractive index, mechanically durable material, with low optical absorption (2.3 eV bandgap [12]) that satisfies waveguiding criteria for some of the defect centres in diamond. Another recent approach is to use diamond resonators fabricated on a SiO<sub>2</sub> substrate with SU8 spot-size converters extending the diamond guides for end-fire injection via lensed fibre [2,4,13-15]. This approach gives a low input loss (1 dB/facet), a waveguide propagation loss of 0.34 dB cm<sup>-1</sup> and an index difference that gives the majority mode overlap within the diamond structure. Another method whereby suspended diamond windows are fabricated for subsequent patterning and transfer from a rigid diamond frame has been demonstrated by utilising a CVD overgrowth technique that shows very good uniformity [16,17]. Other diamond photonic devices have also been fabricated, most notably, diamond nanopillars that show optimal coupling of the pillar mode with native NV emissions [18,19] and 2D photonic crystal structures in diamond with cavity modes close to the zero phonon lines of the most promising colour centres (NV<sup>-</sup> and SiV<sup>-</sup>) [15,20-24]. Angled etching of bulk diamond chips masked by Si/SiO<sub>2</sub> to create suspended structures such as photonic crystals or microresonators have also shown great potential for

\* Corresponding author at: Institute of Photonics, University of Strathclyde, Technology and Innovation Centre, University of Strathclyde, 99 George St., Glasgow G1 1RD, United Kingdom of Great Britain and Northern Ireland.

E-mail address: [paul.hill@strath.ac.uk](mailto:paul.hill@strath.ac.uk) (P. Hill).

<https://doi.org/10.1016/j.diamond.2018.07.020>

Received 19 March 2018; Received in revised form 4 July 2018; Accepted 23 July 2018

Available online 26 July 2018

0925-9635/© 2018 The Authors. Published by Elsevier B.V. This is an open access article under the CC BY license

(<http://creativecommons.org/licenses/by/4.0/>).

colour centre integration [25–30]. Common challenges in most of these works however are in overcoming the severe constraints on circuit integration owing to the limited dimensions ( $\sim\text{mm}^2$ ) of available electronic grade diamond and also with the potential for scaling. Here we propose the fabrication of thin single-crystal diamond membranes using dry etching, that can be transferred onto established photonic circuitry using liquid mediated capillary bonding. A target thickness of diamond is chosen such that it has an increased flexibility whilst remaining robust to minimal handling during transfer. This promotes deformation of the diamond over the device it has to be bonded with. By this approach established fabrication methods can be used for large wafer-scale devices where the diamond is transferred afterwards as a passive component over the required devices. In this work a  $1\ \mu\text{m}$  thick SC diamond membrane was fabricated and transferred onto Si ring resonator devices. Silicon was chosen as a platform for diamond integration as it provides low-loss, highly confining waveguide devices that are well understood and could be used for non-linear applications. This technique can however be used with any planar waveguide technology, such as GaN which has a refractive index more closely matching that of diamond at wavelengths for  $\text{NV}^-$  colour-centre emissions.

## 2. Device design & fabrication

The Silicon devices in this work were fabricated on a silicon on insulator (SOI) wafer with a 220 nm core layer on a  $2\ \mu\text{m}$  buried oxide layer. The waveguides were designed to be 500 nm wide and were patterned using a 200 nm thick e-beam curable, silica-like, hydrogen silesquioxane (HSQ) epoxy. SU8 resist was used for spot size conversion tapers between the guides and external injection fibre. The ring resonators were designed to have a bend radius of 50  $\mu\text{m}$  in a racetrack geometry to give control of the cross coupling coefficient, i.e. the amount of light that will couple to the resonator from the injection waveguide, using a straight coupling section of 41.2  $\mu\text{m}$  [31]. Devices were prepared with both the HSQ mask in place and HSQ mask removed, to show the effect of mode overlap in the material stack. The devices with the cap removed, were treated using a  $\text{CHF}_3$  reactive ion etch (RIE) which etches the  $\text{SiO}_2$  substrate also - thus the Si devices were left on a plinth of the substrate which is shown in Fig. 1. Standard single mode silicon waveguides at telecommunication wavelengths have an effective index larger than that of diamond thus confining the mode more strongly to the former. Finite difference eigenmode (FDE) simulations (Fig. 1) were used to show this whilst also highlighting that an increasing thickness of diamond membrane had negligible effect on the mode overlap between the two materials. As such, the thickness of diamond was instead dictated by the requirement of membrane flexibility to promote larger areas of bonding to the target device. The confinement of the modal power was simulated for three distinct cases, in each case the fundamental transverse electric (TE) mode at a

wavelength  $1.535\ \mu\text{m}$  was calculated. The cases were as follows, the silicon device alone with the HSQ cap; the diamond bonded to the silicon, buffered with the HSQ cap; and finally the diamond bonded to a device with the HSQ removed using RIE. These three cases are depicted in the mode simulations shown in Fig. 1. The simulations showed that for the Silicon device with its HSQ cap present there was a 71% confinement of the modal power within the Si waveguide. This dropped slightly when bonded with diamond to 69% and confinement to the diamond was shown to be less than 1% of the power. For the devices where the HSQ cap had been removed before the diamond was bonded, a 71% modal power confinement to the Si was found but an increase to 13% confinement was observed within the diamond. The diamond membranes in this work were fabricated using Element 6's commercially available electronic grade SC diamond chips with dimensions  $4 \times 4 \times 0.3\ \text{mm}^3$ . The chips were laser diced and mechanically polished into 8 separate samples with approximate dimensions and roughness of  $2 \times 2 \times 0.03\ \text{mm}^3$  and 2 nm r.m.s. respectively. The diamond plates were cleaned in a solution of  $\text{H}_2\text{SO}_4:\text{H}_2\text{O}_2$  with a ratio of 3:1 (Piranha) to remove any organic contaminants and then thinned using an  $\text{ArCl}_2$  inductively coupled plasma (ICP) RIE [32] to  $1\ \mu\text{m}$  thickness at their thinnest for increased flexibility. The diamond etch rate was approximately 65 nm/min and showed a reduction in surface roughness to  $< 1\ \text{nm}$  r.m.s. as has been reported previously for this etch process [32]. Monitoring of the diamond thickness was achieved by white light optical profiling (vertical scanning interferometry). The resultant diamond profile was wedged as is common using this fabrication method [33], showing an approximately 4  $\mu\text{m}$  thickness difference across a sample length of 2 mm after polishing. Measurements taken intermediately between staged etches showed a variation of  $< 0.2\ \mu\text{m}$  in the wedge between the start and end of the thinning process. It was found that the thinner end of the diamond membrane more readily deformed over the devices with larger areas bonded than that of the thicker end. The diamond film was integrated with the target silicon devices by using a liquid mediated capillary bonding method. The target device was prepared with a droplet of isopropyl alcohol and the diamond brought into contact and transferred from a wetted corner of cleanroom wipe. Capillary forces as the liquid evaporates brings the membrane into close contact with the device promoting adhesion. Having been pre-thinned to a target thickness of around  $1\ \mu\text{m}$  at its thinnest end, and with care in alignment, the diamond membrane deforms over the devices as shown schematically in Fig. 2. Nothing other than the capillary forces detailed were used in adhering the diamond to the silicon device.

## 3. Membrane integration with photonic devices

To probe the quality of this interface a number of complementary techniques were used: scanning electron microscopy (SEM), analysis of

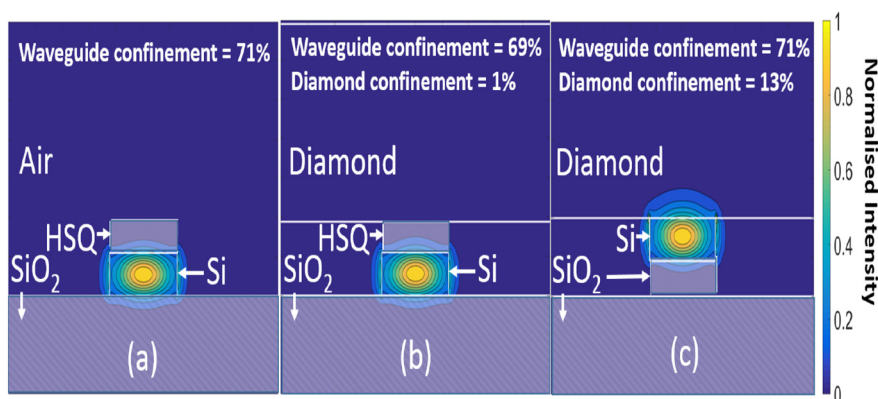


Fig. 1. Cross-sectional mode simulations showing the TE modal power distribution at a wavelength of  $1.535\ \mu\text{m}$  for the three cases of: (a) as fabricated Si device (with HSQ), (b) Si device with diamond bonded and a HSQ buffering cap, and (c) Si device bonded with diamond where the buffering cap is removed. The HSQ cap in (a) and (b) is 200 nm thick and the  $\text{SiO}_2$  plinth in (c) is 200 nm also.

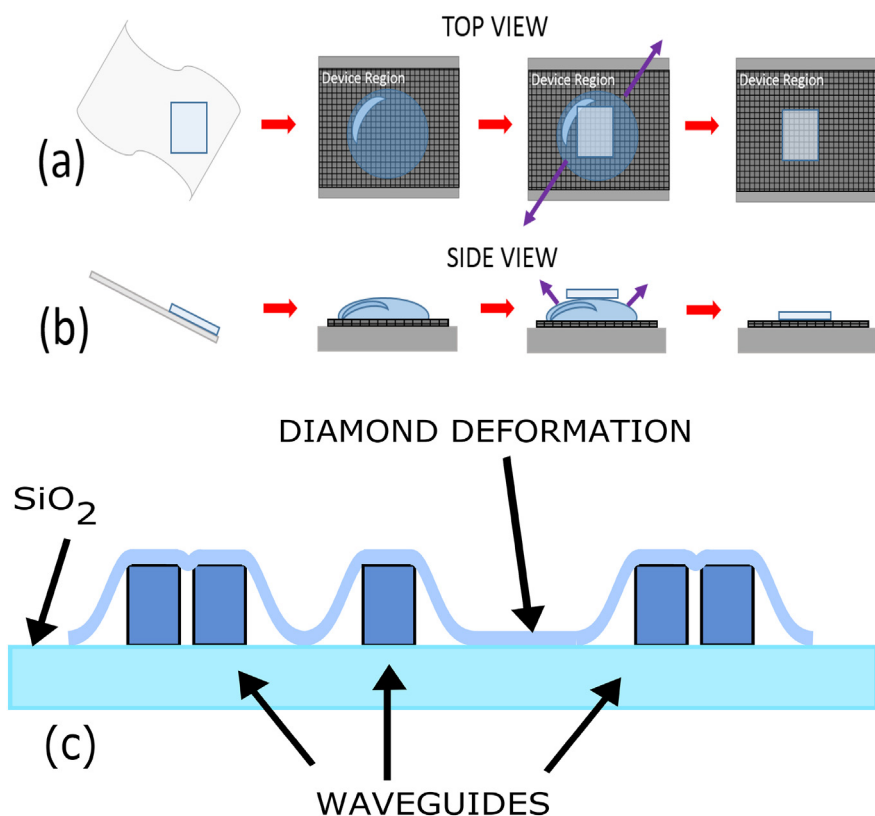


Fig. 2. (a) and (b) are schematics of the diamond membrane bonding procedure onto a processed silicon photonic chip, from a top and side view respectively. Bonding of the materials is facilitated by capillary action bringing the surfaces into contact. (c) A cross sectional schematic of how the diamond membrane conforms over and bonds with the target Si device.

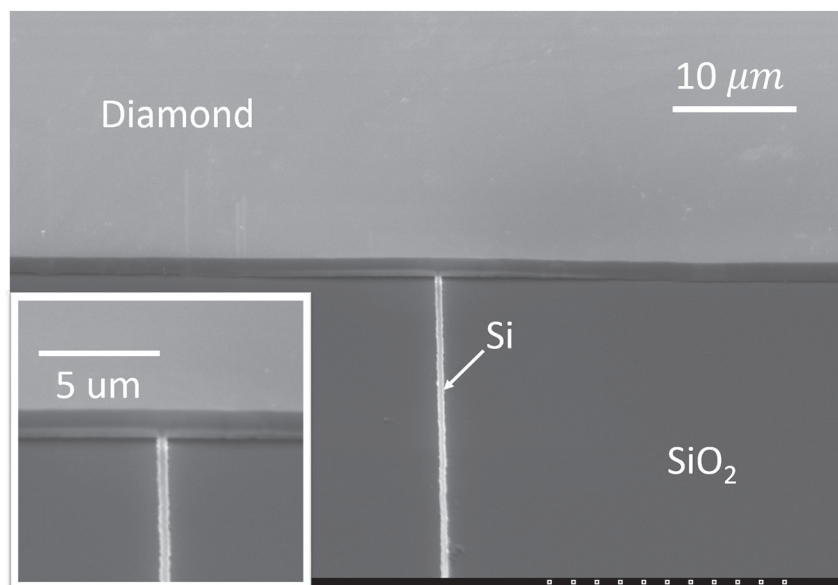


Fig. 3. An oblique-view SEM image showing the bonding of a 1 μm diamond membrane to a Si bus waveguide; it can be seen that the diamond conforms back to and contacts with the substrate within a few micrometres. Inset: Enlarged image at the site of the interface showing the gap between the membrane and substrate.

white light interference patterns, and optical transmission spectra. SEM images were taken to directly observe the deformation with the devices from a stage-tilted view directed towards one of the resonator's bus waveguides as shown in Fig. 3. It can be seen that there is planar contact between the diamond and the top of the Si waveguide as well as contact with the silica substrate approximately 10 μm either side of the device. This shows a good diamond-silicon interface and demonstrates a minimum pitch at which devices could be spaced before full deformation of the diamond to the substrate would occur - in this case devices that were spaced approximately < 20 μm apart would prevent a

diamond deformation large enough for contact with the substrate. Bonding over straight waveguides such as this gave consistent results. SEM is however unsuitable for investigating the interface at the site of the resonator due to the opacity of diamond using this technique. Analysis of optical interference fringes was therefore used instead to map the membrane height across the device. Intimate contact between the waveguide and the diamond membrane can be inferred from this mapping as shown in Fig. 4. Interference patterns can be seen due to constructive or destructive interference of light reflected from the sample surface and the air-diamond interface. Assuming a collimated

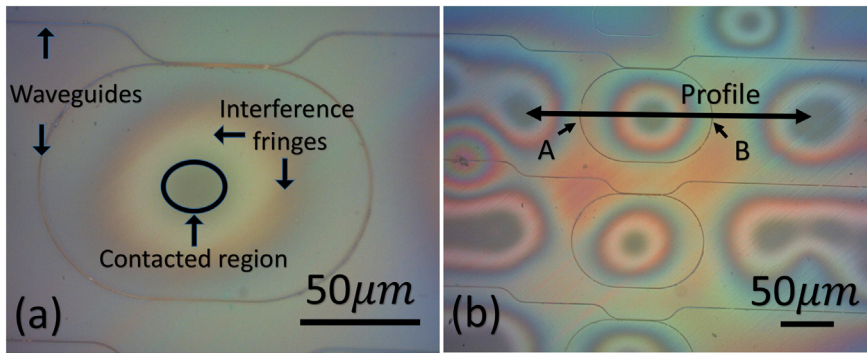


Fig. 4. (a) An optical image of a diamond membrane bonded over a Si resonator device showing interference fringes, a contacted region, and waveguides. (b) Optical image showing the line profile on which fringe analysis was conducted to calculate the height profile over the Si device, where A and B point to either end of the waveguide resonator. (c) A height profile calculated from the fringe intensity over the line profile as shown in (b) with the black lines signifying the waveguide positions of the racetrack labelled again as A and B.

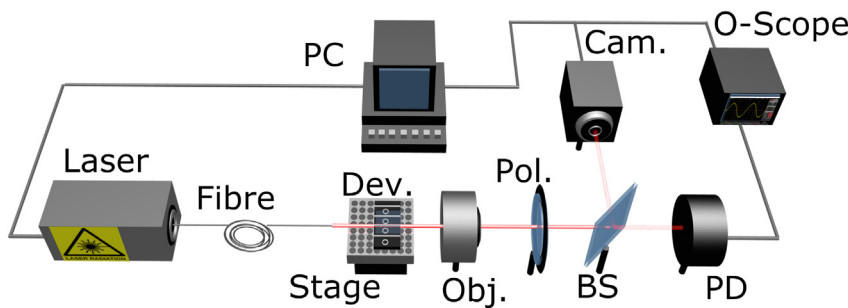
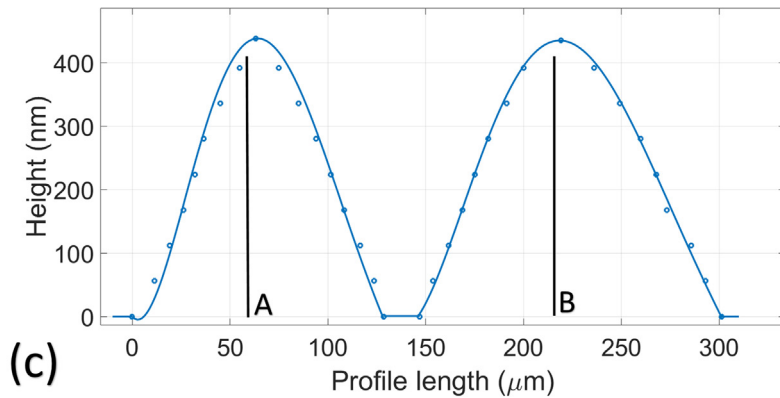


Fig. 5. A schematic of the end-fire rig used to optically measure the silicon devices before and after the bonding of thin diamond membranes. A tunable laser injected through some polarisation maintaining fibre is coupled to the end facet of a device and the emissions are collected from the exit facet using an objective. The collected light is focused through a polariser onto a photodetector and infrared camera via a beam splitter.

monochromatic light source we can calculate the height of the membrane separation from the device substrate using the wavelength of the light and the number of interference fringes counted from the contact point of the diamond and silica substrate. Height values,  $d$ , were calculated for each maxima and minima point of the interference fringes as  $d = n\frac{\lambda}{2}$ , where  $n$  is an integer number. Additionally, points at the fringe full-width-half-maxima were used to calculate height values equal to  $m\frac{\lambda}{8}$ , where  $m$  is an odd integer number. This data can be seen in Fig. 4 which also shows an approximate height morphology using interpolation between the known points; the black vertical lines denote the positions of the Si waveguides. The calculated height profile shows a central contacted region within the racetrack with the height of the membrane located directly above the waveguides varying with the asymmetry of the bond. The height of the membrane then reaches a maximum over a position that may not correspond to the position of the waveguides as is demonstrated in Fig. 4. As the diamond across the bus waveguide only requires deformation across one axis in this case, the material bonds back to the substrate over distances of  $\sim 10 \mu\text{m}$ . In the case of the racetrack resonator the diamond is required to deform over two axes limiting the local gradient with complex dependencies on membrane thickness and the locations of surrounding surface-contacted regions.

#### 4. Optical probe measurements

The optical quality of the bond for use in integrated optical applications was also investigated. To do this we used an end-fire rig with a lensed single mode fibre and coupled it to the end facet of a bus waveguide for a resonator bonded beneath the diamond. A schematic of the optical setup is shown in Fig. 5. All of the measurements reported were taken from an all-pass ring resonator with characteristics defined in Section 2 earlier and transmission spectra taken at telecommunication wavelengths. By curve fitting the transmission spectra shown in Fig. 7 to the analytical model of an all-pass ring resonator [34], values for coupling coefficients, group index values, and distributed losses could be extracted. The power transmission intensity is described by the following equation:

$$T = \frac{I_{\text{pass}}}{I_{\text{input}}} = \frac{a^2 - 2ra \cos \phi + r^2}{1 - 2ar \cos \phi + (ra)^2} \quad (1)$$

where  $a$  is the single-pass amplitude transmission, and defined in terms of the power attenuation coefficient ( $\alpha$ ) of the system as follows:  $a^2 = \exp(-\alpha L)$ .  $r$  is the amplitude self-coupling coefficient and its complimentary parameter is the amplitude cross-coupling coefficient defined as  $k$ . For a lossless system,  $r^2 + k^2 = 1$  and  $k^2 = \kappa$  the power

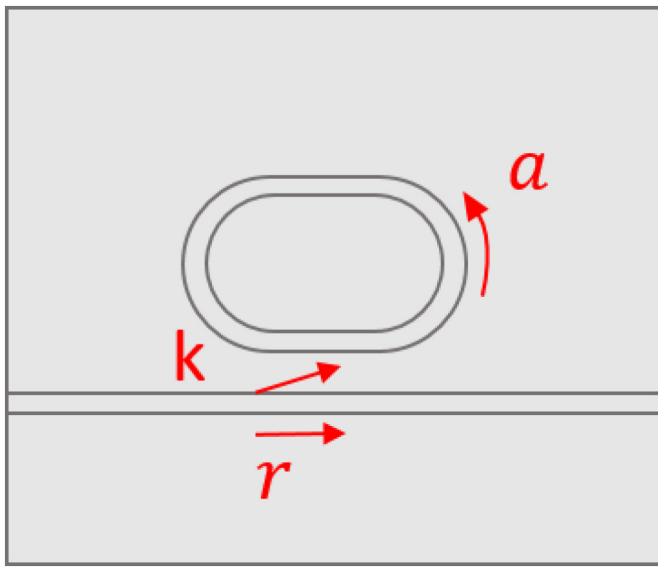


Fig. 6. Schematic of a racetrack resonator showing power cross coupling, transmission, and loss parameters.

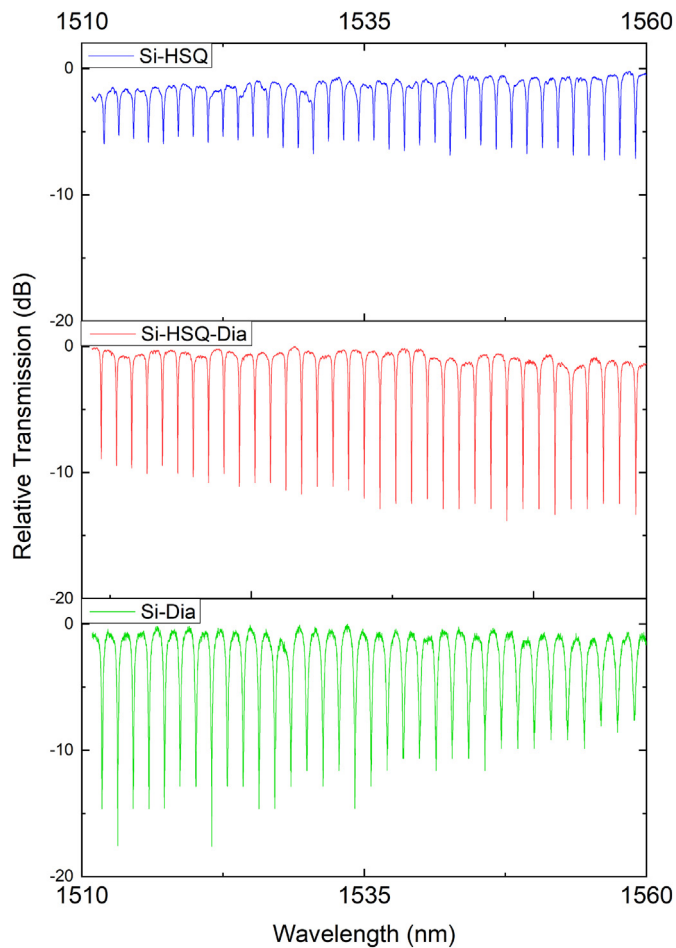


Fig. 7. The normalised transmission spectra for (a) the as-fabricated Si device and when bonded with the diamond pre (b) and post (c) removal of the HSQ mask cap.

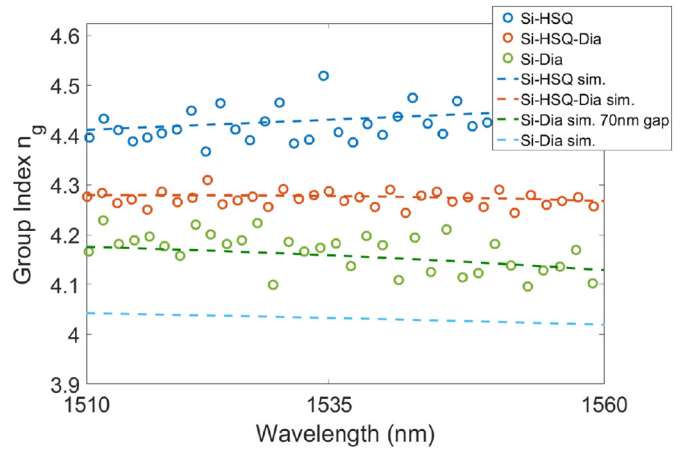


Fig. 8. Extracted, and simulated group index values for the Si ring resonator alone, and when bonded with the 1  $\mu\text{m}$  diamond membrane with and without an HSQ cap. The measured results show a group index shift and gradient in agreement with the simulated values.

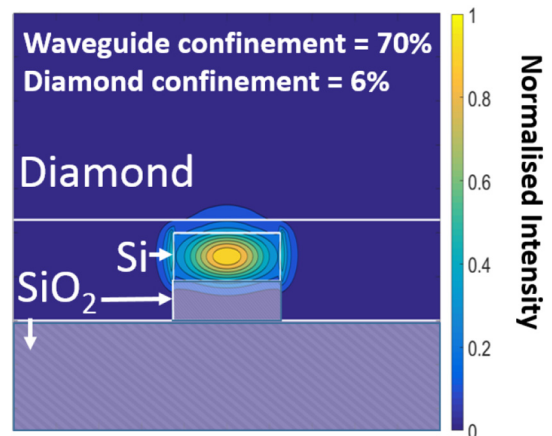


Fig. 9. A cross-sectional mode simulation showing the TE modal power distribution at a wavelength of 1.535  $\mu\text{m}$  for a diamond membrane 70 nm above a Si waveguide with no HSQ cap.

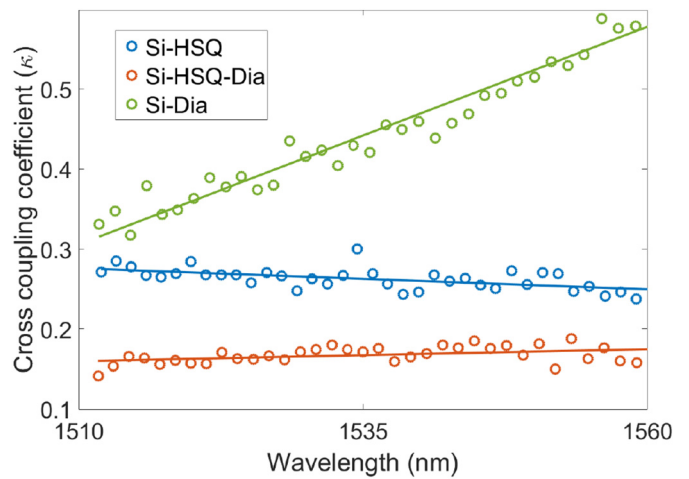


Fig. 10. Cross coupling coefficients for the cases of, as fabricated Si device, and bonded to a diamond membrane with and without the HSQ cap used to pattern the device.

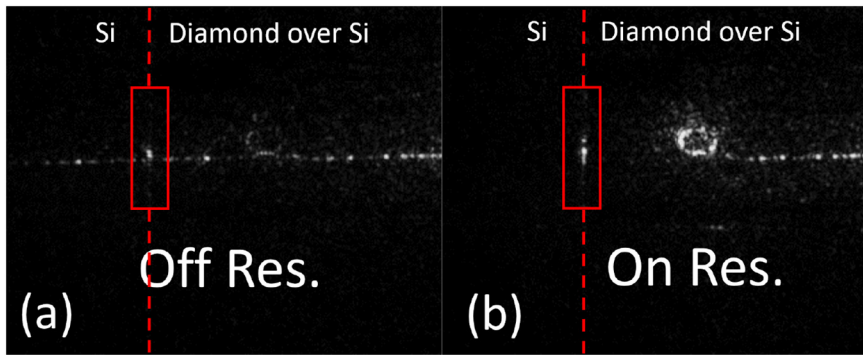


Fig. 11. (a) A top scattering image of a 1  $\mu\text{m}$  diamond membrane bonded to a Si ring resonator off resonance. The red dashed line marks where the edge of the diamond is, and the red box highlights the scattering at this edge. (b) The resonator was tuned into resonance, and again with the red lines and box highlighting the edge of the diamond and scattering respectively. (For interpretation of the references to colour in this figure legend, the reader is referred to the web version of this article.)

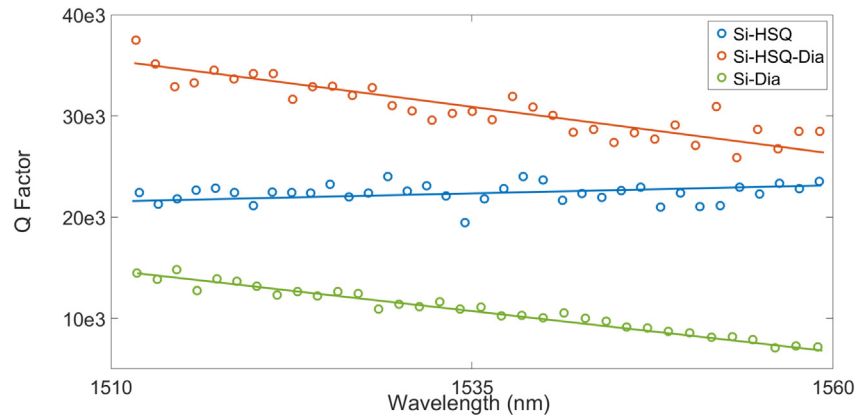


Fig. 12. Loaded Q-Factor values for the cases of a silicon device alone, and bonded with diamond with and without the HSQ cap used to pattern the device.

cross-coupling coefficient -  $a$ ,  $r$ , and  $k$  are depicted in Fig. 6.  $\phi$  is the single-pass phase shift, which is the product of the propagation constant and round trip length,  $\beta$  and  $L$  respectively. The measurement data is fitted to the analytical solution using a least squares method, with  $\kappa$  and  $\alpha$  as free parameters. The group index ( $n_g = n - \lambda_0 \frac{dn}{d\lambda_0}$ ), and the Q factor ( $Q = \frac{f_0}{\Delta f}$ ) can also be calculated from the measured resonant wavelengths and linewidths. The free spectral range is the wavelength spacing between adjacent resonances and is approximated by the equation,  $\frac{\lambda_0^2}{n_g L}$ , where  $\lambda_0$  is the wavelength of light,  $n_g$  is the group index, and  $L$  is the length for 1 round trip of the cavity. The measurements were taken for three different cases detailed earlier to demonstrate an increasing mode interaction with the diamond and the transmission spectra are shown in Fig. 7. From the spectra in Fig. 7 it can be seen that the free spectral range differs between the cases and therefore so does the resulting group index which is shown in Fig. 8. It can be seen from the plot that the group index measurements match that of the FDE model calibrated to the as-fabricated Si waveguide case. In the case of the diamond bonded to the Si devices with the HSQ cap present, the group index measurements shift downwards and are also in agreement with simulations. The gradient of the group index is also seen to change from a positive to negative trend when bonded with the diamond as the simulations predicted. In the case for the diamond bonded to the device with the cap removed, the group index is reduced further but does not reach the simulated values. The measured results of the resonator do not match the simulated group index values for a hybrid diamond-silicon device due to varying degrees of contact across the racetrack resonator. This is in agreement with analysis of the optical image discussed earlier in Section 3. The deformation of the diamond membrane over the resonator device, which has a complex surrounding geometry as shown in Fig. 4, has a contact point that is off-centre and interference fringes that are asymmetric. As a result the diamond-silicon contact is

not fully consistent around the resonator. The result of this non-trivial surface geometry is equivalent to a diamond membrane with an average air gap in the order of 10s of nanometres and thus a less than simulated modal overlap, with a higher measured group index. A simulation of an average 70 nm air gap between the diamond and Si interface over the full resonator shows reasonable matching with the experimental results. To compare this case with the earlier confinement simulations in Fig. 1 a corresponding TE mode calculation at a wavelength of 1.535  $\mu\text{m}$  with the 70 nm gap present is shown in Fig. 9 where the confinement to the Si device is 70% and the diamond 6%. A second property of the resonator that allows assessment of the diamond-silicon interface is the power cross coupling coefficient and is shown in Fig. 10. This is a dimensionless value used to characterise the interaction of the resonator with the bus waveguide. In Fig. 1 it can be seen that in the case of the diamond bonded with the HSQ cap still in place the confinement has been shown not to change greatly, however Fig. 10 shows a reduction in power cross coupling coefficient. This can be explained by the effective index of the two interfaced materials, the device now clad with diamond rather than air. The presence of the diamond reduces the overall effective index difference between the bus waveguide and resonator and thus reduces slightly the cross coupling coefficient compared with that of the as fabricated case. It can also be seen in Fig. 10 that in the presence of the bonded diamond, with no HSQ cap, that the coupling coefficient has increased relative to the as fabricated Si device. Also as the injection wavelength is increased a larger coupling coefficient is observed. Both of these factors are explained by a larger mode overlap between the Si and the diamond membrane which increases with larger wavelengths and facilitates an increased power transfer between the bus guide and resonator. These figures show that the membrane, after the HSQ has been removed, is in close enough proximity to the Si device to facilitate optical interaction between the two. Using an infrared (IR) camera positioned above the hybrid Si-

diamond device, scattered light was observed, with the diamond bonded, whilst the device was on and off resonance shown in Fig. 11. It can be seen that the amount of vertical scattering is not discernibly different when measured from the Si waveguide alone or from the Si waveguide underneath the diamond suggesting the hybrid device had a low additional propagation loss. When the laser is tuned to a wavelength that is resonant with the racetrack cavity, the scattered light at the diamond edge is contrasted more clearly due to a large reduction in propagating light through the bus waveguide. This point source of scattered light at the diamond edge is also not noticeably different to that of the Si device's propagation losses showing that this interface does not add a large amount of optical loss. The added distributed losses of the ring itself which were extracted by the curve fitting method as detailed above, corroborated these findings and showed an added loss of 0.4 dB per round trip. Finally we measured loaded Q-factors for the three cases detailed before and found mean averaged values of 22.3k for the silicon device alone, 30.8k for the Si-HSQ-Dia, and 10.8k for the Si-Dia. The data has been plotted with trend lines in Fig. 12. The wavelength dependent loaded Q-factor is dominated by the inverse relationship with power cross coupling coefficients of each device case.

## 5. Conclusion

In conclusion we have shown that thin, free-standing SC diamond membranes can be integrated with photonic devices fabricated on more mature platforms. The mechanical and optical qualities of the bond were evaluated using SEM, optical interference calculations, and transmission spectra before and after the diamond was bonded. Group index dispersion measurements were conducted and compared with simulated values and found to be in good agreement, demonstrating an optical interaction with the diamond membrane. A low added loss of 0.4 dB per turn was achieved and a Q-factor of around 10k for the hybrid diamond-silicon resonator was found. By choosing relevant host-substrate materials, this integration technique could be used for a wide range of applications spanning several wavelength ranges.

## Acknowledgements

We would like to thank C. Klitis and M. Sorel for providing the silicon devices. The research data associated with this paper are available at: <https://doi.org/10.15129/7da6a6a3-b298-4e4a-b720-94a699017f61>.

## Funding information

This work was supported by the EPSRC [EP/P013597/1], the National Quantum Information Technology Hub [EP/M013243/1], and Fraunhofer UK [EP/L015315/1].

## References

- I. Aharonovich, A.D. Greentree, S. Praver, *Diamond photonics*, *Nat. Photonics* 5 (2011) 397–405.
- P. Latawiec, V. Venkataraman, M.J. Burek, B.J.M. Hausmann, I. Bulu, M. Lončar, On-chip diamond Raman laser, *Optica* 2 (2015) 924.
- F. Gao, J. Van Erps, Z. Huang, H. Thienpont, R.G. Beausoleil, N. Vermeulen, Directional coupler based on single-crystal diamond waveguides, *IEEE J. Sel. Top. Quantum Electron.* 24 (2018) 1–9.
- B.J.M. Hausmann, I. Bulu, V. Venkataraman, P. Deotare, M. Lončar, Diamond nonlinear photonics, *Nat. Photonics* 8 (2014) 369–374.
- M.W. McCutcheon, M. Loncar, Design of a silicon nitride photonic crystal nanocavity with a quality factor of one million for coupling to a diamond nanocrystal, *Opt. Express* 16 (2008) 19136.
- D. Englund, B. Shields, K. Rivoire, F. Hatami, J. Vučković, H. Park, M.D. Lukin, Deterministic coupling of a single nitrogen vacancy center to a photonic crystal cavity, *Nano Lett.* 10 (2010) 3922–3926.
- N. Thomas, R.J. Barbour, Y.C. Song, M.L. Lee, K.M.C. Fu, Waveguide-integrated single-crystalline GaP resonators on diamond, *Opt. Express* 22 (2014) 13555–13564.
- M. Gould, S. Chakravarthi, I.R. Christen, N. Thomas, S. Dadgostar, Y. Song, M.L. Lee, F. Hatami, K.-M.C. Fu, Large-scale GaP-on-diamond integrated photonics platform for NV center-based quantum information, *J. Opt. Soc. Am. B* 33 (2016) B35.
- M. Gould, E.R. Schmidgall, S. Dadgostar, F. Hatami, K.M.C. Fu, Efficient extraction of zero-phonon-line photons from single nitrogen-vacancy centers in an integrated GaP-on-diamond platform, *Phys. Rev. Appl.* 6 (2016) 2–7.
- P.E. Barclay, K.M.C. Fu, C. Santori, A. Faraon, R.G. Beausoleil, Hybrid nanocavity resonant enhancement of color center emission in diamond, *Phys. Rev. X* 1 (2011) 1–7.
- P.E. Barclay, K.M.C. Fu, C. Santori, R.G. Beausoleil, Chip-based microcavities coupled to nitrogen-vacancy centers in single crystal diamond, *Appl. Phys. Lett.* 95 (2009) 93–96.
- M.B. Panish, Temperature dependence of the energy gap in GaAs and GaP, *J. Appl. Phys.* 40 (1969) 163.
- P. Latawiec, V. Venkataraman, A. Shams-Ansari, M. Markham, M. Lončar, Integrated diamond Raman laser pumped in the near-visible, *Opt. Lett.* 43 (2018) 318.
- B.J.M. Hausmann, B. Shields, Q. Quan, P. Maletinsky, M. McCutcheon, J.T. Choy, T.M. Babinec, A. Kubanek, A. Yacoby, M.D. Lukin, M. Loncar, Integrated diamond networks for quantum nanophotonics, *Nano Lett.* 12 (2012) 1578–1582.
- B.J.M. Hausmann, I.B. Bulu, P.B. Deotare, M. McCutcheon, V. Venkataraman, M.L. Markham, D.J. Twitchen, M. Lončar, Integrated high-quality factor optical resonators in diamond, *Nano Lett.* 13 (2013) 1898–1902.
- A.H. Piracha, P. Rath, K. Ganesan, S. Kühn, W.H.P. Pernice, S. Praver, Scalable fabrication of integrated nanophotonic circuits on arrays of thin single crystal diamond membrane windows, *Nano Lett.* 16 (2016) 3341–3347.
- A.H. Piracha, K. Ganesan, D.W.M. Lau, A. Stacey, L.P. McGuinness, S. Tomljenovic-Hanic, S. Praver, Scalable fabrication of high-quality, ultra-thin single crystal diamond membrane windows, *Nanoscale* 8 (2016) 6860–6865.
- T.M. Babinec, B.J. Hausmann, M. Khan, Y. Zhang, J.R. Maze, P.R. Hemmer, M. Lončar, A diamond nanowire single-photon source, *Nat. Nanotechnol.* 5 (2010) 195–199.
- E. Neu, P. Appel, M. Ganzhorn, J. Miguel-Sanchez, M. Lesik, V. Mille, V. Jacques, A. Tallaire, J. Achard, P. Maletinsky, Photonic nano-structures on (111)-oriented diamond, *Appl. Phys. Lett.* 104 (2014) 4.
- J.L. Zhang, S. Sun, M.J. Burek, C. Dory, Y.-K. Tzeng, K.A. Fischer, Y. Kelaita, K.G. Lagoudakis, M. Radulaski, Z.-X. Shen, N.A. Melosh, S. Chu, M. Lončar, J. Vučković, Strongly cavity-enhanced spontaneous emission from silicon-vacancy centers in diamond, *Nano Lett.* 18 (2018) 1360–1365.
- M.J. Burek, C. Meuwly, R.E. Evans, M.K. Bhaskar, A. Sipahigil, S. Meesala, B. Machiels, D.D. Sukachev, C.T. Nguyen, J.L. Pacheco, E. Bielejec, M.D. Lukin, M. Lončar, Fiber-coupled diamond quantum nanophotonic interface, *Phys. Rev. Appl.* 8 (2017) 024026.
- A. Sipahigil, R.E. Evans, D.D. Sukachev, M.J. Burek, J. Borregaard, M.K. Bhaskar, C.T. Nguyen, J.L. Pacheco, H.A. Atikian, C. Meuwly, R.M. Camacho, F. Jelezko, E. Bielejec, H. Park, M. Lončar, M.D. Lukin, An integrated diamond nanophotonics platform for quantum-optical networks, *Science* 354 (2016) 847–850.
- L. Li, T. Schröder, E.H. Chen, M. Walsh, I. Bayn, J. Goldstein, O. Gaathon, M.E. Trusheim, M. Lu, J. Mower, M. Cotlet, M.L. Markham, D.J. Twitchen, D. Englund, Coherent spin control of a nanocavity-enhanced qubit in diamond, *Nat. Commun.* 6 (2015) 6173.
- A. Faraon, C. Santori, Z. Huang, V.M. Acosta, R.G. Beausoleil, Coupling of nitrogen-vacancy centers to photonic crystal cavities in monocrystalline diamond, *Phys. Rev. Lett.* 109 (2012) 033604.
- M.J. Burek, N.P. De Leon, B.J. Shields, B.J. Hausmann, Y. Chu, Q. Quan, A.S. Zibrov, H. Park, M.D. Lukin, M. Lončar, Free-standing mechanical and photonic nanostructures in single-crystal diamond, *Nano Lett.* 12 (2012) 6084–6089.
- I. Bayn, S. Mouradian, L. Li, J.A. Goldstein, T. Schröder, J. Zheng, E.H. Chen, O. Gaathon, M. Lu, A. Stein, C.A. Ruggiero, J. Salzman, R. Kalish, D. Englund, Fabrication of triangular nanobeam waveguide networks in bulk diamond using single-crystal silicon hard masks, *Appl. Phys. Lett.* 105 (2014).
- H.A. Atikian, P. Latawiec, M.J. Burek, Y.-I. Sohn, S. Meesala, N. Gravel, A.B. Kouki, M. Lončar, Freestanding nanostructures via reactive ion beam angled etching, *APL Photonics* 2 (2017) 051301.
- S. Mouradian, N.H. Wan, T. Schröder, D. Englund, Rectangular photonic crystal nanobeam cavities in bulk diamond, *Appl. Phys. Lett.* 111 (2017).
- N.H. Wan, S. Mouradian, D. Englund, Two-dimensional photonic crystal slab nanocavities on bulk single-crystal diamond, *Appl. Phys. Lett.* 112 (2018).
- M.J. Burek, Y. Chu, M.S. Liddy, P. Patel, J. Rochman, S. Meesala, W. Hong, Q. Quan, M.D. Lukin, M. Loncar, High quality-factor optical nanocavities in bulk single-crystal diamond, *Nat. Commun.* 5 (2014) 1–7.
- M.J. Strain, C. Lacava, L. Meriggi, I. Cristiani, M. Sorel, Tunable Q-factor silicon microring resonators for ultra-low power parametric processes, *Opt. Lett.* 40 (2015) 1274.
- C.L. Lee, E. Gu, M.D. Dawson, I. Friel, G.A. Scarsbrook, Etching and micro-optics fabrication in diamond using chlorine-based inductively-coupled plasma, *Diam. Relat. Mater.* 17 (2008) 1292–1296.
- Y. Tao, C. Degen, Facile fabrication of single-crystal-diamond nanostructures with ultrahigh aspect ratio, *Adv. Mater.* 25 (2013) 3962–3967.
- W. Bogaerts, P. de Heyn, T. van Vaerenbergh, K. de Vos, S. Kumar Selvaraja, T. Claes, P. Dumon, P. Bienstman, D. van Thourhout, R. Baets, Silicon microring resonators, *Laser Photonics Rev.* 6 (2012) 47–73.